# Optimization of a Pressure-Swing Adsorption Process Using Zeolite 13X for $CO_2$ Sequestration

**Daeho Ko,[†] Ranjani Siriwardane,[‡] and Lorenz T. Biegler*[,†]**

*Department of Chemical Engineering, Carnegie Mellon University, 5000 Forbes Avenue, Pittsburgh, Pennsylvania 15213, and U.S. Department of Energy, National Energy Technology Laboratory, 3610 Collins Ferry Road, Morgantown, West Virginia 26507*

A pressure-swing adsorption process, which uses zeolite 13X as an adsorbent to recover and sequester carbon dioxide from mixture gas (nitrogen and carbon dioxide), is investigated through dynamic simulation and optimization. The purpose of this paper is to improve the purity of each component by finding optimal values of decision variables with a given power constraint. Langmuir isotherm parameters are calculated from experimental data of zeolite 13X and a general mathematical model consisting of a set of partial differential and algebraic equations and solved in gPROMS. The method of centered finite differences is adopted for the discretization of the spatial domains, and a reduced space SQP method is used for the optimization. As a result, the optimal conditions at cyclic steady state are obtained.

## 1. Introduction

Adsorption processes have been suggested as an alternative to traditional separation processes such as distillation and absorption. Gaseous species are adsorbed preferentially on solid sorbents, and when the adsorbent is saturated, a thermal-swing adsorption (TSA) or a pressure-swing adsorption (PSA) method is employed for the regeneration under the condition of continuous periodic operation. In the PSA process, the adsorbent is regenerated by quickly decreasing the partial pressure of the adsorbate, i.e., reducing the total pressure using a purge gas. With this PSA technology, binary-component and multicomponent gas mixtures are commercially being separated.[1,2] For environmental applications, one of the most promising applications of PSA is to recover and sequester $CO_2$ from flue gas streams. One way to improve the efficiency of the process is to adopt a suitable adsorbent; the other is to find optimal values of design and operating variables of the process. Design variables include the choice of sorbent as well as the bed length and diameter, while operating variables include the feed pressure and operating step times. However, the optimization procedure does not deal with control issues for the PSA process. Here separate control strategies need to be developed in order to stabilize the process and to maintain it at the desired operating points. These are discussed in Bitzer and Zeitz.[3]

In this study we select zeolite 13X as an adsorbent to sequester $CO_2$ and optimize the PSA process because it has a high efficiency of separation and requires low power for $CO_2$ sequestration. Many studies have dealt with the simulation and optimization of adsorption processes. These systems require the solution of partial differential algebraic equations (PDAEs) to model adsorption in each bed, enforcement of periodic boundary conditions to describe cyclic steady states (CSSs), and the determination of optimal design and operating variables. Croft and Levan[4] presented a simulation method for the direct determination and stability analysis of periodic states of adsorption cycles. Similarly, Kvamsdal and Hertzberg[5] investigated different methods to accelerate cyclic steady-state convergence such as Aitken, Muller, and Broyden based updating schemes as well as a damped Newton-based approach. To deal with optimization, Smith and Westerberg[6,7] considered the cyclic operating schedule of a PSA system as a mixed-integer nonlinear program (MINLP) that was simplified to a mixed-integer linear program (MILP); they determined the optimal values of the number of beds, the desired operation, the scheduling of those operations, and the operating conditions.[8] Nilchan and Pantelides[9] proposed the complete discretization (CD) method for the optimization of PSA and rapid PSA (RPSA) processes. A CD, sometimes called simultaneous discretization, that discretizes both the spatial and time domains has been applied to adsorption processes.[9−14] Lewandowski et al.[15] developed a method using neural networks for the simulation and optimization of a PSA process. Jiang et al.[16] optimized a PSA system by using a direct determination method by implementing a Newton-based approach to accelerate convergence for CSSs.

However, little has been published on the optimization of PSA processes using zeolite 13X for $CO_2$ sequestration. This work concentrates on the dynamic simulation and optimization of a bench-scale PSA system with zeolite 13X as the adsorbent, to remove $CO_2$ from mixture gas consisting of $N_2$ and $CO_2$. The feed composition is 15% $CO_2$ and 85% $N_2$. The mathematical model including the adsorption rate, mass balance, and heat balance influenced by adsorption heat has been formulated for a four-step operating PSA cycle (pressurization, adsorption, depressurization, and regeneration) in a single bed, as shown in Figure 1. The selected adsorbent, zeolite 13X, is very good at separating $CO_2$ from the mixture gas consisting of $N_2$ and $CO_2$. Pure gas adsorp-

* Corresponding author. Fax: 412 268 7139. Tel: 412 268 2232. E-mail: lb01@andrew.cmu.edu.

[†] Carnegie Mellon University.

[‡] U.S. Department of Energy, National Energy Technology Lab.

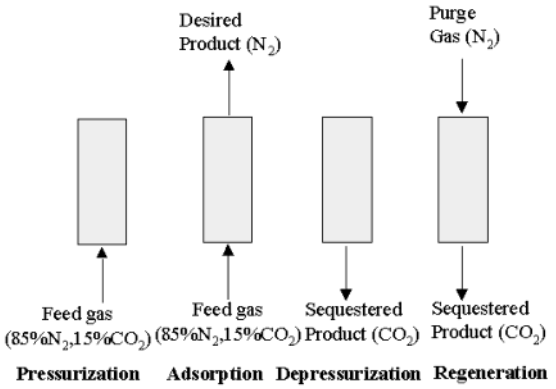


**Figure 1.** Four-step operation of the PSA process.

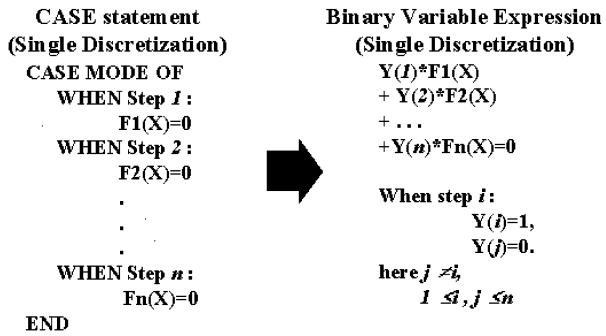


**Figure 2.** Expression of different conditions at each operating step by a binary variable in gPROMS (before version 2.1).

tion isotherm parameters are calculated from experimental data,[17] and the Langmuir equation for mixture gas isotherms is used to describe the competitive adsorption behavior in this work. This study considers the optimization of PSA at CSS by using a single discretization (SD) approach that discretizes just the spatial domain; hybrid features in the gProms allow switching of the boundary conditions associated with modeling of different operating steps in the cycle. As demonstrated, the adopted methodology is more reliable than the CD method for the optimization of cyclic adsorption processes in the gProms[19,20] modeling system.

The next section summarizes the modeling and optimization strategy. Here we present the process model, the constraints for the optimization problem, and the discretization method. Section 3 then presents the numerical results for the optimization problem, while section 4 concludes the paper.

## 2. Process Description and Model

We consider a PSA cycle with beds packed with zeolite 13X as an adsorbent and operated with four steps: pressurization, adsorption, depressurization, and desorption (Figure 3). During the pressurization step, high-pressure feed gas consisting of 85% $N_2$ and 15% $CO_2$ at ambient temperature is supplied to the bottom of the bed. During the adsorption step, $CO_2$ is adsorbed on a fixed adsorbent (zeolite 13X), $N_2$ is obtained as a product at the top of the bed, and the high-pressure feed gas enters the bed continuously as in the pressurization step. During the depressurization step, $CO_2$ starts being recovered. The desorption step also obtains $CO_2$ at the bottom of the bed, and $N_2$ at ambient pressure is employed as a purge gas. The target process of our current work is bench scale, and the design specifications and simulation conditions are listed in Table 1.

**2.1. Model Equations.** The following assumptions are used for the PSA modeling and simulations.

1. All of the gases follow the ideal gas law.

2. The axial pressure gradient is expressed by Darcy's law.

3. The radial variation of variables such as temperature, pressure, and concentration can be neglected.

4. The superficial velocity is constant through the bed during adsorption and desorption steps.

5. Transport and physical properties are independent of the temperature.

6. Competitive adsorption behaviors are described by the Langmuir equation for mixture gas.

7. The adsorption rate is approximated by a linear driving force (LDF) expression.

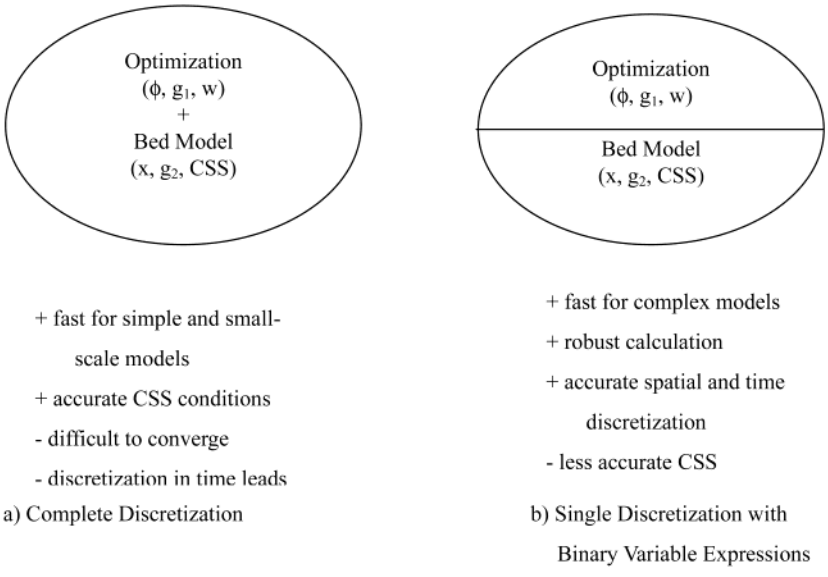


**Figure 3.** Optimization approaches for cyclic adsorption processes.

**Table 1. Basic Simulation Conditions of the PSA Model**

| parameter | value |
|---|---|
| bed length ($L$) | 1 m |
| bed radius ($R_{bed}$) | $1.1 \times 10^{-2}$ m |
| pore diameter ($D_{pore}$) | $1.0 \times 10^{-9}$ m |
| particle radius ($R_{particle}$) | $1.0 \times 10^{-3}$ m |
| bed density ($\rho_{bed}$) | $1.06 \times 10^{3}$ kg/m$^3$ |
| wall density ($\rho_{wall}$) | $7.8 \times 10^{3}$ kg/m$^3$ |
| bed void ($\epsilon_{bed}$) | 0.348 |
| particle density ($\rho_{particle}$) | $1.87 \times 10^{3}$ kg/m$^3$ |
| $R$ | 8.314 J/mol/K |
| heat capacity of a solid ($C_{ps}$) | 504 J/kg/K |
| heat-transfer coefficient of the wall ($U_{wall}$) | 60 J/m$^2$/K/s |
| feed temperature ($T_{feed}$) | 313.15 K |
| wall temperature ($T_{wall}$) | 313.15 K |
| feed pressure ($P_{feed}$) | 2.56 atm |
| purge pressure ($P_{purge}$) | 1.1 atm |
| atmospheric pressure ($P_{atm}$) | 1 atm |
| adsorption gas velocity ($u_{feed}$) | $2.6 \times 10^{-2}$ m/s |
| regeneration gas velocity ($u_{reg}$) | $-$d.3 $\times 10^{-3}$ m/s |
| pressurization time ($t_P$) | 10 s |
| adsorption time ($t_A$) | 50 s |
| depressurization time ($t_{DP}$) | 10 s |
| regeneration time ($t_R$) | 50 s |

**Table 2. Values of Parameters of the Langmuir Isotherm**

| | $CO_2$ | $N_2$ |
|---|---|---|
| $m_1$ | $-2\,580\,917.266\,327\,981$ | $-9.3717 \times 10^{-6}$ |
| $m_2$ | $-284.046\,688\,8$ | $1.031 \times 10^{-7}$ |
| $m_3$ | $8\,641\,161.673\,977\,85$ | $-2.135 \times 10^{-10}$ |
| $m_4$ | $-0.039\,301\,094$ | 0 |
| $n_1$ | $-0.466\,430\,081\,578\,747$ | $4.270 \times 10^{-7}$ |
| $n_2$ | $-290.086\,874\,2$ | $1.289 \times 10^{-7}$ |
| $n_3$ | $0.555\,476\,570\,130\,020\,7$ | $-8.29 \times 10^{-2}$ |
| $n_4$ | $-0.035\,944\,714\,946\,618$ | $3.23 \times 10^{2}$ |

Based on the above assumptions, the mass balance equation of each component $i$ is given by

$$-D_x \frac{\partial^2 y_i}{\partial z^2} + \frac{\partial y_i}{\partial t} + u \frac{\partial y_i}{\partial z} + \frac{RT}{P} \frac{1-\epsilon_{bed}}{\epsilon_{bed}} \rho_{particle} \left( \frac{\partial q_i}{\partial t} - y_i \sum_{i=1}^{n} \frac{\partial q_i}{\partial t} \right) = 0 \quad (1)$$

where $D_x$ is the dispersion coefficient (m$^2$/s), $i$ is the component index for $CO_2$ ($i = 1$) and $N_2$ ($i = 2$), $y_i$ is the gas-phase mole fraction of component $i$, $z$ is the axial position (m), $u$ is the superficial gas velocity (m/s), $R$ is the universal gas constant (J/mol/K), $T$ is the gas temperature within the bed (K), $P$ is the total pressure (Pa), $\epsilon_{bed}$ is the bed void, $\rho_{particle}$ is the particle density (kg/m$^3$), and $q_i$ is the solid-phase concentration (mol/kg).

The adsorption rate can be represented by the LDF model:

$$\frac{\partial q_i}{\partial t} = \frac{15 D_e}{R_{particle}} (q_i^* - q_i) \quad (2)$$

where $q_i^*$ is the amount of adsorption of component $i$ in the equilibrium state of the mixture, $D_e$ is the effective diffusivity (m$^2$/s), and $R_{particle}$ is the particle radius (m).

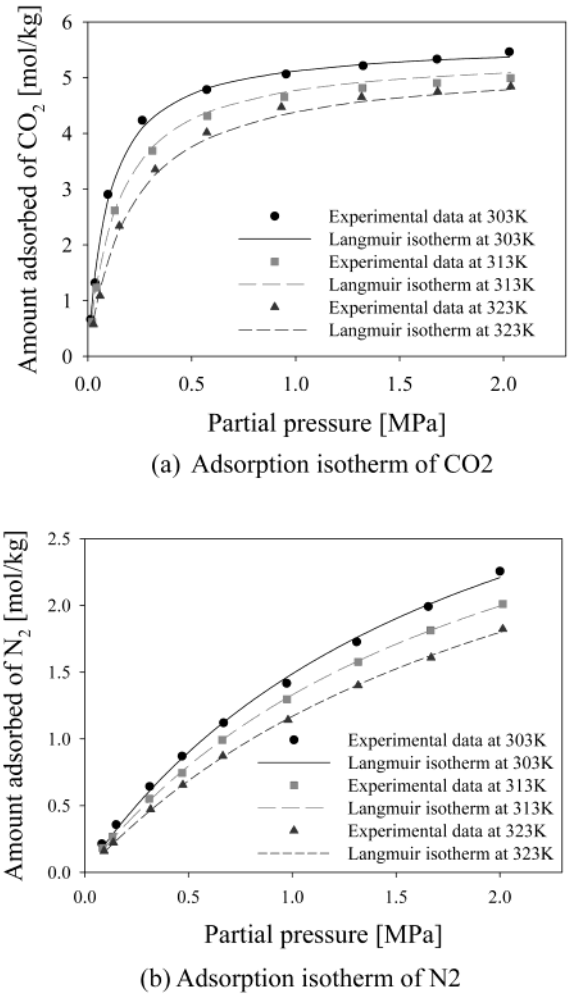


**Figure 4.** Adsorption isotherms at different temperatures on zeolite 13X.

The following Langmuir isotherm can describe the adsorption equilibrium.

$$q_i^* = \frac{a_i P_i}{1 + \sum_{i=1}^{n} b_i P_i} \quad (3)$$

The isotherm parameters are functions of temperature and are expressed by

$$a_{CO_2} = m_1 \exp(m_2 T) + m_3 \exp(m_4 T) \quad (4a)$$

$$b_{CO_2} = n_1 \exp(n_2 T) + n_3 \exp(n_4 T) \quad (4b)$$

$$a_{N_2} = m_1 + m_2 T + m_3 T^2 + m_4 T^3 \quad (4c)$$

$$b_{N_2} = n_1 + n_2\{1 - \exp[n_3(n_4 - T)]\} \quad (4d)$$

The values of these parameters are calculated by employing a nonlinear regression method and are listed in Table 2. Figure 4 shows that the experimental data[17] have a good agreement with the Langmuir isotherms obtained in this study. Moreover, Figure 4 shows that the adsorbent (zeolite 13X) has a very high selectivity of $CO_2$ over $N_2$.

The following energy balance for the column is necessary, because the bed is nonisothermal in the bulk separation.

$$(\epsilon_t \rho_{gas} C_{pg} + \rho_{bed} C_{ps}) \frac{\partial T}{\partial t} + \rho_{gas} C_{pg} \epsilon_{bed} u \frac{\partial T}{\partial z} - K_L \frac{\partial^2 T}{\partial z^2} - \rho_{bed} \sum_{i=1}^{n} \Delta H_i \frac{\partial q_i}{\partial t} + \frac{2h_i}{R_{bed}} (T - T_{wall}) = 0 \quad (5)$$

where $\epsilon_t$ is the total void fraction, $\rho_{gas}$ is the gas density (kg/m$^3$), $C_{pg}$ is the heat capacity of the gas (J/kg/K), $\rho_{bed}$ is the bed density (kg/m$^3$), $C_{ps}$ is the heat capacity of the adsorbent (J/kg/K), $K_L$ is the effective axial thermal conductivity (J/m/s/K), $\Delta H_i$ is the isosteric heat of adsorption (J/mol) of component $i$, $R_{bed}$ is the bed radius (m), $h_i$ is the heat-transfer coefficient (J/m$^2$/s/K), and $T_{wall}$ is the column wall temperature (K). The pressure drop can be described by Darcy's law[18] with the assumption of the laminar flow of gas through the bed

$$\frac{\partial P}{\partial z} = -\frac{180\mu(1-\epsilon_{bed})^2 u}{\epsilon_{bed}{}^3 D_{particle}{}^2} \quad (6)$$

where $\mu$ is the gas viscosity (kg/m/s) and $D_{particle}$ is the particle diameter (m). The isosteric heat of adsorption is calculated by using the Clausius−Clapeyron equation as the follows:

$$\left[\frac{\mathrm{d} \ln P}{\mathrm{d}(1/T)}\right]_q = -\frac{\Delta H}{R} \quad (7)$$

The boundary conditions for the PSA operation are shown in Table 3. Table 4 lists the mole flux variables (Feed, Product, Exhaust, and PurgeFeed) to calculate the performances such as purities and recoveries. Consequently, the purities and recoveries of $CO_2$ ($i$ = 1) and $N_2$ ($i$ = 2) are given by

$$\mathrm{Purity}_{CO_2} = \frac{\mathrm{Exhaust}_{CO_2}}{\sum_{i=1}^{n} \mathrm{Exhaust}_i} \quad (8)$$

$$\mathrm{Purity}_{N_2} = \frac{\mathrm{Product}_{N_2}}{\sum_{i=1}^{n} \mathrm{Product}_i} \quad (9)$$

$$\mathrm{Recovery}_{CO_2} = \frac{\mathrm{Exhaust}_{CO_2}}{\mathrm{Feed}_{CO_2}} \quad (10)$$

$$\mathrm{Recovery}_{N_2} = \frac{\mathrm{Product}_{N_2}}{\mathrm{Feed}_{N_2}} \quad (11)$$

The power is calculated by

$$\mathrm{Power} = \frac{\gamma}{\gamma - 1} R T_{feed} \left[\left(\frac{P_{feed}}{P_{atm}}\right)^{(\gamma-1)/\gamma} - 1\right] u_{feed} \pi R_{bed}{}^2 \frac{P_{feed}}{R T_{feed}} \quad (12)$$

where $P_{atm}$ is the atmospheric pressure (1 atm).

**Table 3. Boundary Conditions of Each Operating Step (Here $T_{Feed}$ = 313.15 K)**

| pressurization | adsorption | depressurization | regeneration |
|---|---|---|---|
| $y_i\|_{z=0} = y_{f,i}$ | $y_i\|_{z=0} = y_{f,i}$ | $\left.\frac{\partial y_i}{\partial z}\right\|_{z=0} = 0$ | $\left.\frac{\partial y_i}{\partial z}\right\|_{z=0} = 0$ |
| $\left.\frac{\partial y_i}{\partial z}\right\|_{z=L} = 0$ | $\left.\frac{\partial y_i}{\partial z}\right\|_{z=L} = 0$ | $\left.\frac{\partial y_i}{\partial z}\right\|_{z=L} = 0$ | $y_{CO_2}\|_{z=L} = 0$, $y_{N_2}\|_{z=L} = 1$ |
| $P\|_{z=0} = P_{feed}$ | $P\|_{z=0} = P_{feed}$ | $P\|_{z=0} = P_{purge}$ | $P\|_{z=0} = P_{purge}$ |
| $\left.\frac{\partial P}{\partial z}\right\|_{z=L} = 0$ | $\left.\frac{\partial P}{\partial z}\right\|_{z=L} = 0$ | $\left.\frac{\partial P}{\partial z}\right\|_{z=L} = 0$ | $\left.\frac{\partial P}{\partial z}\right\|_{z=L} = 0$ |
| $T\|_{z=0} = T_{feed}$ | $T\|_{z=0} = T_{feed}$ | $\left.\frac{\partial T}{\partial z}\right\|_{z=0} = 0$ | $\left.\frac{\partial T}{\partial z}\right\|_{z=0} = 0$ |
| $\left.\frac{\partial T}{\partial z}\right\|_{z=L} = 0$ | $\left.\frac{\partial T}{\partial z}\right\|_{z=L} = 0$ | $\left.\frac{\partial T}{\partial z}\right\|_{z=L} = 0$ | $\left.\frac{\partial T}{\partial z}\right\|_{z=L} = 0$ |
| $u\|_{z=0} = u_{feed}$ | $u\|_{z=0} = u_{feed}$ | $u\|_{z=0} = u_{reg}$ | $u\|_{z=0} = u_{reg}$ |
| $u\|_{z=L} = 0$ | $u\|_{z=L} = u_{feed}$ | $u\|_{z=L} = 0$ | $u\|_{z=L} = u_{reg}$ |

The average performance of the PSA is evaluated by the following criteria:

$$\mathrm{Purity}_{CO_2,Ave} = \frac{\int_{t_P+t_A}^{t_{cycle}} \mathrm{Purity}_{CO_2}\, \mathrm{d}t}{t_{DP} + t_R} \quad (13)$$

$$\mathrm{Purity}_{N_2,Ave} = \frac{\int_{t_P}^{t_P+t_A} \mathrm{Purity}_{N_2}\, \mathrm{d}t}{t_A} \quad (14)$$

$$\mathrm{Recovery}_{CO_2,Ave} = \frac{\int_{t_P+t_A}^{t_{cycle}} \mathrm{Recovery}_{CO_2}\, \mathrm{d}t}{t_{DP} + t_R} \quad (15)$$

$$\mathrm{Recovery}_{CO_2,Ave} = \frac{\int_{t_P}^{t_P+t_A} \mathrm{Recovery}_{N_2}\, \mathrm{d}t}{t_A} \quad (16)$$

where $t_P$ is the pressurization time, $t_A$ is the adsorption time, $t_{DP}$ is the depressurization time, $t_R$ is the regeneration time, and $t_{cycle}$ is the cycle time that is the sum of the each operating step time ($t_{cycle} = t_P + t_A + t_{DP} + t_R$).

This mathematical formulation consists of partial differential equations, algebraic equations, and integral equations for the mass balance, the Langmuir isotherm equation, and the performance measure, respectively. In addition, the boundary conditions at the end of the bed change abruptly and periodically during the operating cycle. In this study, the method of lines (MOL)[21] and finite difference method (FDM) are adopted to convert the PDAE system to a differential algebraic equation (DAE) system. For dynamic simulation, integration over time is performed by a DAE integrator in gProms based on backward differentiation formulas (BDF). The main advantage of this method is that the DAE integrator automatically controls the integration error for all variables.[22]

**2.2. CSS.** The following statement specifies the CSS of the PSA process: *The spatial bed profiles must be identical at the beginning and end of the cycle.* That is to say, the initial profiles are generally determined by eq 17a−c that defines CSS.

$$y_i|_{t=0} = y_i|_{t=t_{cycle}} \quad (17a)$$

$$q_i|_{t=0} = q_i|_{t=t_{cycle}} \quad (17b)$$

$$T|_{t=0} = T|_{t=t_{cycle}} \quad (17c)$$

**Table 4. Mole Flux Variables at Each Operating Step**

| pressurization | adsorption | depressurization | regeneration |
|---|---|---|---|
| $\frac{\partial(\text{Feed}_i)}{\partial t} = \frac{uP_i}{RT}\Big\vert_{z=0}$ | $\frac{\partial(\text{Feed}_i)}{\partial t} = \frac{uP_i}{RT}\Big\vert_{z=0}$ | $\frac{\partial(\text{Feed}_i)}{\partial t} = 0$ | $\frac{\partial(\text{Feed}_i)}{\partial t} = 0$ |
| $\frac{\partial(\text{Product}_i)}{\partial t} = 0$ | $\frac{\partial(\text{Product}_i)}{\partial t} = \frac{uP_i}{RT}\Big\vert_{z=L}$ | $\frac{\partial(\text{Product}_i)}{\partial t} = 0$ | $\frac{\partial(\text{Product}_i)}{\partial t} = 0$ |
| $\frac{\partial(\text{Exhaust}_i)}{\partial t} = 0$ | $\frac{\partial(\text{Exhaust}_i)}{\partial t} = 0$ | $\frac{\partial(\text{Exhaust}_i)}{\partial t} = -\frac{uP_i}{RT}\Big\vert_{z=0}$ | $\frac{\partial(\text{Exhaust}_i)}{\partial t} = -\frac{uP_i}{RT}\Big\vert_{z=0}$ |
| $\frac{\partial(\text{PurgeFeed}_i)}{\partial t} = 0$ | $\frac{\partial(\text{PurgeFeed}_i)}{\partial t} = 0$ | $\frac{\partial(\text{PurgeFeed}_i)}{\partial t} = 0$ | $\frac{\partial(\text{PurgeFeed}_i)}{\partial t} = -\frac{uP_i}{RT}\Big\vert_{z=L}$ |

For the spatial profiles of the variables in $z$ ($y_i$, $q_i$, and $T$), this study employed the following parametrization to describe the initial conditions for these profiles and capture their desired shapes.

$$q_i|_{t=0} = k_{a,q_i} + \frac{k_{b,q_i}}{1 + \exp\left[-\frac{z - k_{c,q_i}}{k_{d,q_i}}\right]} \quad (18a)$$

$$y_i|_{t=0} = k_{a,y_i} + \frac{k_{b,y_i}}{1 + \exp\left[-\frac{z - k_{c,y_i}}{k_{d,y_i}}\right]} \quad (18b)$$

$$T|_{t=0} = k_{a,T} + \frac{k_{b,T}}{1 + \exp\left[-\frac{z - k_{c,T}}{k_{d,T}}\right]} \quad (18c)$$

The ranges of the parameters ($k_a$, $k_b$, $k_c$, and $k_d$) in the optimization are decided by considering the profiles of $q|_{t=t_{cycle}}$, $y|_{t=t_{cycle}}$, and $T|_{t=t_{cycle}}$ at CSS, resulting from successive substitution (SS) from the first cycle to the 500th cycle (≈CSS), and the values of the parameters are determined from the optimization to satisfy the CSS conditions (eq 17a−c). The basic conditions for the simulation of the SS method are listed in Table 1. This work employs the following constraints for the optimization at CSS, and the bed profiles at initial time are determined through the optimization, with the following bounds on the variables: $k_{a,q_1} \in [0.1, 10]$, $k_{b,q_1} \in [-5, -0.1]$, $k_{c,q_1} \in [-1, -0.001]$, $k_{d,q_1} \in [0.05, 4]$, $k_{a,q_2} \in [0.001, 1]$, $k_{b,q_2}$, $k_{d,y_2} \in [0.01, 10]$, $k_{c,q_2}$, $k_{c,y_2} \in [-0.1, -0.001]$, $k_{d,q_2} \in [0.05, 0.4]$, $k_{a,y_2} \in [0, 0.9]$, $k_{b,y_2}$, $k_{d,T} \in [0.01, 5]$, $k_{a,T} \in [300, 315]$, $k_{b,T} \in [0.5, 3]$, and $k_{c,T} \in [-0.5, -0.05]$. The CSS conditions are given as constraints in the optimization model, and the following equations are used to determine CSS for the optimization.

$$|(\int_{0|+}^{L|-} y_i \, dz)_{t=0} - (\int_{0|+}^{L|-} y_i \, dz)_{t=t_{cycle}}| \le \epsilon \quad (19a)$$

$$|(\int_{0}^{L} q_i \, dz)_{t=0} - (\int_{0}^{L} q_i \, dz)_{t=t_{cycle}}| \le \epsilon \quad (19b)$$

$$|(\int_{0|+}^{L|-} T \, dz)_{t=0} - (\int_{0|+}^{L|-} T \, dz)_{t=t_{cycle}}| \le \epsilon \quad (19c)$$

$$y_1|_{t=0} + y_2|_{t=0} = 1 \quad (19d)$$

where $\epsilon$ is a small tolerance ($\epsilon \sim 10^{-3}$). Because of the parametrization of the bed profiles (18) and the constraints (19), the converged CSS may not be as accurate as the approach in work by Jiang et al.[16] This stems from the fact that their profiles can be specified freely at each node point in the MOL and the CSS conditions are satisfied at each node point, where the CSS conditions are derived from the MOL. Nevertheless, through considerable evaluation, we found that this approach yields both reasonable and efficient solutions for optimization in the framework of gPROMS. Figures 5−7 show the CSS behaviors of the variables ($q$, $y$, $T$) obtained by the optimization cases in this study.

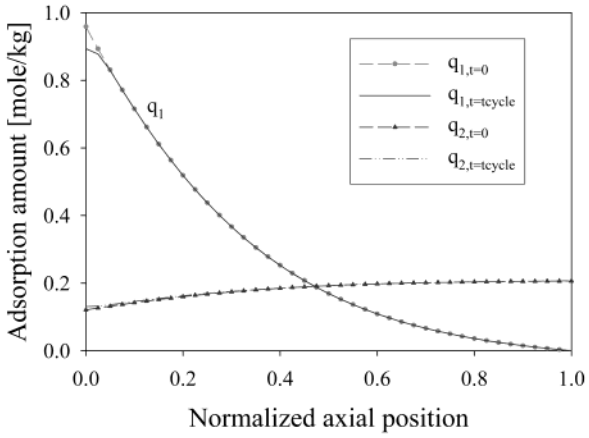


(a) First optimization case

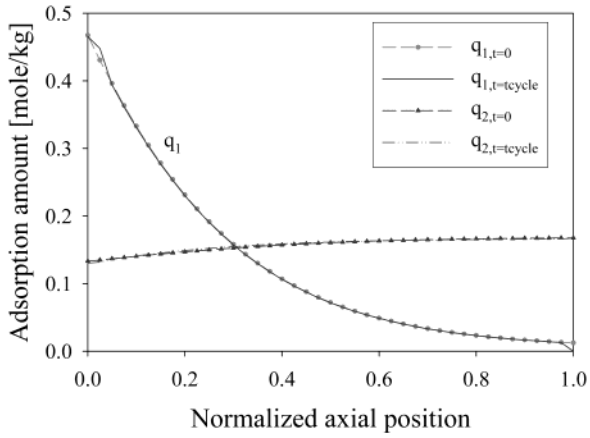


(b) Second optimization case

**Figure 5.** CSS behaviors of solid-phase concentration ($q_1$, adsorption amount of $CO_2$; $q_2$, adsorption amount of $N_2$).

**2.3. Overall Optimization Strategy.** For the optimization of a periodic adsorption process, CSS requires the initial and final conditions of a cycle to be identical. Traditionally CSS has been determined through the SS

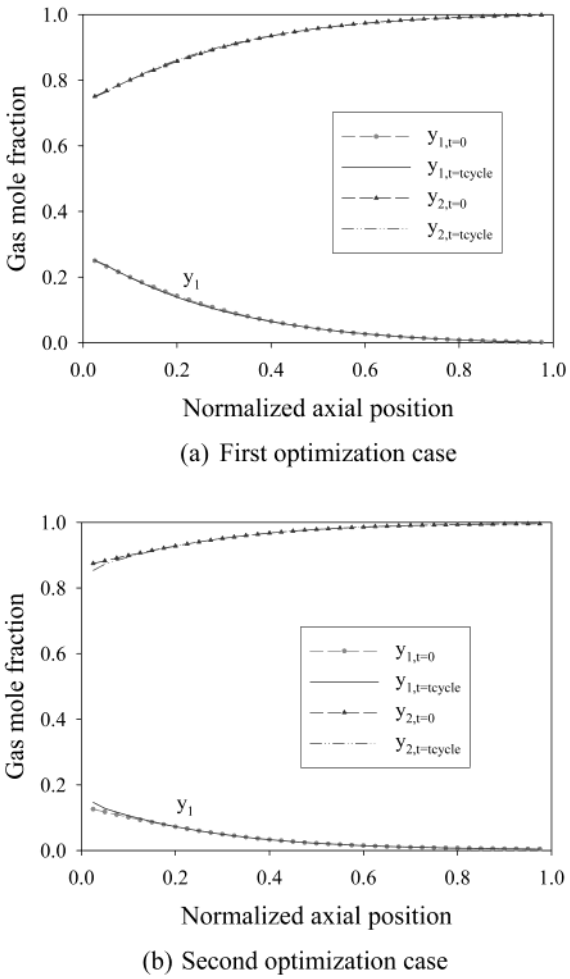


**Figure 6.** CSS behaviors of gas-phase mole fraction ($y_1$, mole fraction of $CO_2$; $y_2$, mole fraction of $N_2$).

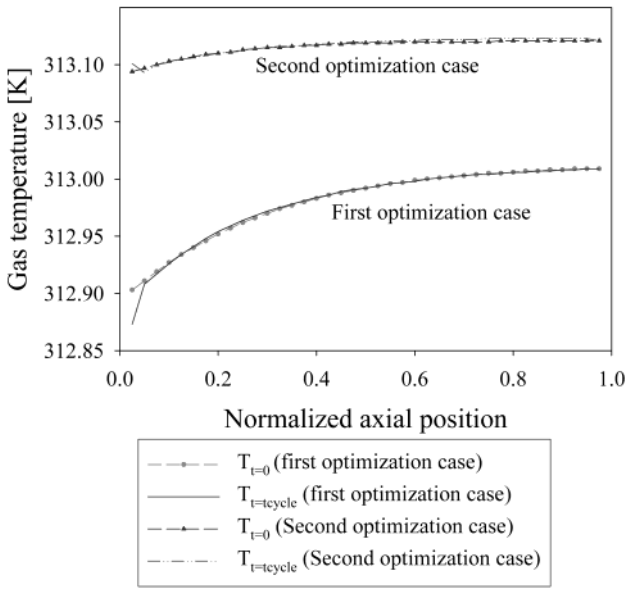


**Figure 7.** CSS behaviors of gas temperature.

scheme. The SS scheme is the repeated dynamic simulation of each step over the PSA cycle. This corresponds to the way that PSA units operate in practice to obtain CSS. With SS the number of simulation cycles to reach CSS may be very large, and the rate of convergence on CSS may be enhanced by making use of a quasi-Newton or Newton method. The Newton-type approach is desirable if it reduces iteration numbers significantly compared to the SS scheme. However, this Newton-type method often requires substantially increased computational time for each iteration.[4,6] Moreover, it is much more difficult to optimize a cyclic operating system, especially in a spatially distributed system, than to simulate the system. The spatially distributed model can be lumped into a differential and algebraic equation (DAE) system to solve the difficulty. Optimization of DAE systems has been extensively studied and can be solved by employing a sequential or simultaneous approach. The simultaneous CD approach attains a significant improvement in computational time, even though the model size is comparatively large. However, in simulation and optimization, the CD model is more difficult to converge for complex models than a SD model, which discretizes only a spatial domain, and the simulation of the CD model can produce different results because SD models employ variable time steps (continuous time domain) while here the CD model adopts a fixed time grid (discrete time domain). In section 3 we discuss the characteristics of the CD method and compare the optimization with the SD method using an RPSA example. Instead, we adopt an SD approach for the PSA system optimization and CSS is determined directly as a constraint in the optimization model.

Based on the dynamic simulation, the optimization is performed by the dynamic optimizer, gOPT in gProms.[19,20] This converts the optimization problem to a nonlinear programming (NLP) problem using a control vector parametrization (CVP) technique, with a successive quadratic programming (SQP) algorithm as implemented in the SRQPD code.[23] The procedure for this work is as follows:

(1) Formulate the model using the SD approach,

(2) Describe the different boundary conditions at each operating step by using binary variables instead of a Case statement. (See Table 3. Case statements are not supported for optimization in gPROMS before version 2.1, although they are supported for more recent versions, where BVEs are not necessary.)

(3) Add the CSS condition (19) as the inequality constraint.

(4) Perform the optimization using gOPT in gProms.

The main advantages of this method are as follows: (i) the model is robust for the simulation and optimization calculations; (ii) the model is easier to converge and initialize and more reliable to solve than CD models for simulation and optimization, and (iii) performance values calculated from optimal decision variables through optimization are the same as those through simulation.

The simulation time of the binary variable model is similar to that of the general model using case statements on a Pentium III Linux machine with dual CPU (800 MHz), and the simulation results are exactly the same. The BVE method based on the SD approach is described and compared to that of the CD approach in Figures 2 and 3 and in section 3.

## 3. Optimization Results

To illustrate the benefits of the SD approach, we first present a comparison with the CD approach on a small RPSA process for oxygen recovery from air. Following this example, we consider two optimization cases for $CO_2$ sequestration.

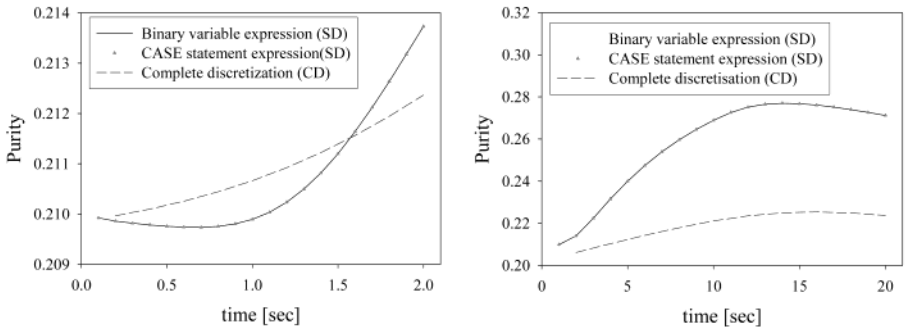


(a) Purity when $t_P = t_{DP} = 1$sec (b) Purity when $t_P = t_{DP} = 10$sec

**Figure 8.** Comparison of simulation results between SD and CD.

**Table 5. RPSA Model Equations[12]**

| | | |
|---|---|---|
| mass balance | | $\epsilon_t\left[\frac{1}{t_{cycle}}\right]\frac{\partial C_i}{\partial t} + \rho_{bed}\left[\frac{1}{t_{cycle}}\right]\frac{\partial q_i}{\partial t} = -\left[\frac{1}{L_{bed}}\right]\frac{\partial (uC_i)}{\partial z} + D_z\left[\frac{1}{L_{bed}^2}\right]\frac{\partial^2 C_i}{\partial z^2}, \quad \forall z \in (0, \hat{L}_{bed}), t \in (0, \hat{t}_{cycle})$ |
| adsorption rate | | $\left[\frac{1}{t_{cycle}}\right]\frac{\partial q_i}{\partial t} = k_{i,z}(q_i^* - q_i), \quad \forall z \in [0, \hat{L}_{bed}], t \in [0, \hat{t}_{cycle}]$ |
| linear Langmuir isotherm | | $q_i^* = m_i C_i RT, \quad \forall z \in [0, \hat{L}_{bed}], t \in [0, \hat{t}_{cycle}], i = 1, ..., n$ |
| Darcy's law | | $\left[\frac{1}{L_{bed}}\right]\frac{\partial P}{\partial z} = \frac{180\mu(1-\epsilon_{bed})^2}{d_p^2 \epsilon_{bed}^3}u, \quad \forall z \in [0, \hat{L}_{bed})$ |
| at the feed end | pressurization | $C_i = y_i\frac{P|_{z=0}}{RT}, \quad P|_{z=0} = P_{feed}$ |
| | depressurization | $\left[\frac{1}{L_{bed}}\right]\frac{\partial C_i}{\partial z}\Big\|_{z=0} = 0, \quad P|_{z=0} = P_{purge}$ |
| at the product end | | $\left[\frac{1}{L_{bed}}\right]\frac{\partial C_i}{\partial z}\Big\|_{z=\hat{L}_{bed}} = 0, \quad v_z = \frac{Q}{A}\frac{P_{atm}}{P}$ |
| purity of $O_2$ | | $\text{Purity} = \left.\frac{uC_{O_2}}{\sum_{i=1}^{2} v_z C_i}\right\|_{z=\hat{L}_{bed}}$ |
| power | | eq 12 |

**Table 6. Total CPU Time (s) for Simulation of Each Case**

| operating step time condition | SD | | |
|---|---|---|---|
| | Case model | BVE model | CD model |
| $t_P = t_{DP} = 1$ s | 0.320 | 0.360 | 0.120 |
| $t_P = t_{DP} = 10$ s | 0.500 | 0.540 | 0.110 |

**3.1. Comparison of the CD and Binary Variable Expression (BVE) Methods.** The CD and SD are compared by taking an RPSA example process,[24] which separates oxygen from the air, with operating steps consisting of pressurization and depressurization. The model for this example is given in Table 5. We performed the simulation in gPROMS by using both CD and SD methods. Operating step change conditions are expressed by binary variables or the Case statement in the SD method and by time domain discretization in the CD method. Table 6 shows the calculation time of these simulations. The computation of the CD method is much faster than that of the SD approach, and the Case expression and the BVE have similar calculation speeds in the simulation. However, as shown in Figure 8, the CD approach has results different from those of the SD method, because of a less accurate discretization. On the other hand, the simulation result of the BVE model is the same as that of the Case statement expression.

This work treats the optimization of only the first cyclic pass of the RPSA process in order to check the difference of the BVE and CD models. The optimization formulation is

$$\text{Min Power/Purity} \tag{20}$$

Subject to

$$0.1 \text{ m} \le L_{bed} \le 1.5 \text{ m} \tag{21a}$$

$$1 \text{ atm} \le P_{feed} \le 10 \text{ atm} \tag{21b}$$

$$0.1 \text{ s} \le t_P \le 10 \text{ s} \tag{21c}$$

$$0.1 \text{ s} \le t_{DP} \le 10 \text{ s} \tag{21d}$$

$$\text{Purity}_j \le \text{Purity}_{t_{cycle}} \le 1 \qquad j = 1, 2, \text{or } 3 \tag{21e}$$

Here, we consider

$$\text{Purity}_1 = 0.35, \quad \text{Purity}_2 = 0.3, \quad \text{or Purity}_3 = 0.25$$

Table 7 compares the optimization results of the two models. Though the optimization with the CD model is faster than that with the BVE model, it is more difficult

**Table 7. Optimization Results of the BVE and CD Models in Each Purity Constraint**

| model type | purity constraint | $L$ (m) | $P_{feed}$ (atm) | $t_P$ (s) | $t_{DP}$ (s) | purity | power (J/s) | objective (J/s) | total CPU time (s) |
|---|---|---|---|---|---|---|---|---|---|
| BVE (SD) | purity > 0.35 | 0.286 | 2.47 | 10 | 0.1 | 0.35 | 2.549 | 7.282 | 10.7 |
| | purity > 0.30 | 0.231 | 1.86 | 10 | 0.1 | 0.30 | 1.254 | 4.180 | 15.1 |
| | purity > 0.25 | 0.183 | 1.35 | 9.92 | 0.1 | 0.25 | 0.420 | 1.681 | 9.9 |
| CD | purity > 0.30 | error in optimization | | | | | | | |
| | purity > 0.25 | error in optimization | | | | | | | |
| | purity > 0.35 | 1.500 | 4.08 | 4.36 | 7.28 | 0.25 | 7.053 | 28.213 | 7.0 |

to converge reliably, as is seen in Table 7. Consequently, the BVE model has an advantage over the CD model in the optimization of cyclic adsorption processes.

**3.2. PSA Optimization for $CO_2$ Sequestration.** We now consider two optimization cases for the sequestration of $CO_2$. The objective function and constraints of each case are the same except for the "Power" constraint. The objective function is to increase the purities of $N_2$ and $CO_2$. The optimization model is the following:

$$\text{Max Purity}_{N_2} + \text{Purity}_{CO_2} \tag{22}$$

Subject to

$$0.15\ \text{m} \le L \le 2\ \text{m} \tag{23a}$$

$$1.7\ \text{atm} \le P_{feed} \le 20\ \text{atm} \tag{23b}$$

$$0.7\ \text{atm} \le P_{purge} \le 1.1\ \text{atm} \tag{23c}$$

$$0.001\ \text{m/s} \le u_{feed} \le 0.02\ \text{m/s} \tag{23d}$$

$$-0.01\ \text{m/s} \le u_{reg} \le -0.001\ \text{m/s} \tag{23e}$$

$$1\ \text{s} \le t_P \le 10\ \text{s} \tag{23f}$$

$$49\ \text{s} \le t_A \le 990\ \text{s} \tag{23g}$$

$$1\ \text{s} \le t_{DP} \le 10\ \text{s} \tag{23h}$$

$$49\ \text{s} \le t_R \le 990\ \text{s} \tag{23i}$$

$$\text{Purity}_{CO_2} \ge 15\% \tag{23j}$$

$$\text{Purity}_{N_2} \ge 85\% \tag{23k}$$

$$\text{Required Power} \le \text{Power (J/s)} \tag{23l}$$

Equations 1−12, 18a−c, and 19a−d and equations of Tables 3 and 4 are also used.

The above $\text{Purity}_i$ ($i = CO_2$ and $N_2$) constraints given by eqs 8 and 9 are calculated at the end of a given cycle.

In the first case, the power constraint is given by eq 23l for Power = 0.6 J/s. The optimal results of the first case are listed in Table 8. The optimal feed pressure is 1.84 atm, the optimal purge pressure is 1.10 atm, the optimal bed length is 0.98 m, the optimal gas velocities during adsorption and regeneration are $1.28 \times 10^{-2}$ and −0.001 m/s, respectively, and the optimal cycle time is 205.673 s. Consequently, the average performance is calculated from the optimal decision variables. The computation time for the optimization is 3177.9 CPU s on a Pentium III Linux machine with dual 800 MHz CPU.

In the second case, the required power is set to be less than 0.5 J/s (eq 23a). The optimal decision values are shown in Table 9. The optimal bed length is 0.91 m, the optimal feed pressure is 1.70 atm, the optimal purge pressure is 0.88 atm, the gas velocities of adsorption and desorption are $1.35 \times 10^{-2}$ and $-1.05 \times 10^{-3}$ m/s, respectively, and the optimal cycle time is 308.605 s. The average purities and recoveries of $CO_2$ and $N_2$ are also obtained as shown in Table 7. The total CPU time for the optimization is 5273.3 CPU s on the same machine (Pentium III Linux machine with dual CPU (800 MHz)).

Judging from extensive sensitivity studies about the optimum solutions, the required power is affected only by the feed pressure and adsorption gas velocity and not by the bed length, purge pressure, and operating step times; it increases as the adsorption gas velocity and feed pressure increase. The purity of $CO_2$ is improved when the purge operating times (the depressurization and regeneration times) increase. The purity of $CO_2$ decreases as the purge pressure and linear gas velocity of the regeneration step increase. The recovery

**Table 8. Optimization Results of the First Case (Power ≤ 0.6 J/s)[a]**

| variable | result |
|---|---|
| bed length ($L$) | 0.976 21 m |
| feed pressure ($P_{feed}$) | 1.842 27 atm |
| purge pressure ($P_{purge}$) | 1.099 54 atm |
| linear gas velocity of adsorption step ($u_{feed}$) | $1.2834 \times 10^{-2}$ m/s |
| linear gas velocity of desorption step ($u_{reg}$) | $-1.00 \times 10^{-3}$ m/s |
| pressurization time ($t_P$) | 10.00 s |
| adsorption time ($t_A$) | 49.00 s |
| depressurization time ($t_{DP}$) | 10.00 s |
| regeneration time ($t_R$) | 136.678 s |
| average purity of $CO_2$ ($\text{Purity}_{CO_2,Ave}$) | 0.244 188 |
| average recovery of $CO_2$ ($\text{Recovery}_{CO_2,Ave}$) | 0.094 673 |
| average purity of $N_2$ ($\text{Purity}_{N_2,Ave}$) | 0.999 648 796 |
| average recovery of $N_2$ ($\text{Recovery}_{N_2,Ave}$) | 0.754 791 |
| power | 0.6 J/s |

[a] Total CPU time for optimization is 3177.9 s on a Pentium III Linux machine with dual CPU (800 MHz) [SRQPD optimizer statistics]. Number of optimization iterations: 82. Number of line search steps: 136.

**Table 9. Optimization Results of the Second Case (Power ≤ 0.5 J/s)[a]**

| variable | result |
|---|---|
| bed length ($L$) | 0.909 834 m |
| feed pressure ($P_{feed}$) | 1.7 atm |
| purge pressure ($P_{purge}$) | 0.881 645 atm |
| linear gas velocity of adsorption step ($u_{feed}$) | $1.350\ 39 \times 10^{-2}$ m/s |
| linear gas velocity of desorption step ($u_{reg}$) | $-1.046 \times 10^{-3}$ m/s |
| pressurization time ($t_P$) | 9.381 21 s |
| adsorption time ($t_A$) | 56.3994 s |
| depressurization time ($t_{DP}$) | 1 s |
| regeneration time ($t_R$) | 241.824 s |
| average purity of $CO_2$ ($\text{Purity}_{CO_2,Ave}$) | 0.149 254 |
| average recovery of $CO_2$ ($\text{Recovery}_{CO_2,Ave}$) | 0.074 332 |
| average purity of $N_2$ ($\text{Purity}_{N_2,Ave}$) | 0.997 653 |
| average recovery of $N_2$ ($\text{Recovery}_{N_2,Ave}$) | 0.791 963 |
| power | 0.5 J/s |

[a] Total CPU time for optimization is 5273.3 s on a Pentium III Linux machine with dual CPU (800 MHz) [SRQPD optimizer statistics]. Number of optimization iterations: 125. Number of line search steps: 242.

of $CO_2$ increases, as the purge pressure, regeneration gas velocity, and purge step times increase, and it decreases accordingly as the feed pressure, adsorption gas velocity, and feeding operation times (the pressurization and adsorption times) increase. Though the purity of $N_2$ is hardly affected by the decision variables and is over 99%, it is slightly enhanced when the bed length, feed pressure, and pressurization time increase. The purity of $N_2$ deteriorates when the adsorption gas velocity increases. The recovery of $N_2$ decreases as the bed length, feed pressure, adsorption gas velocity, and pressurization time increase and the adsorption time decreases.

The optimal results might be affected by the initial guess and bounds of the parameters ($k_a$, $k_b$, $k_c$, and $k_d$) for the optimization, determined by considering the simulation results (first cycle $\sim$ CSS) based on the conditions in Table 1. Because the optimization tolerance is 0.001, the optimal decision variables were found even if the objective value still increased with a very small step. Therefore, it is very important to determine the optimization tolerance and the initial conditions reasonably, as was confirmed in this work.

## 4. Conclusions

A mathematical model of the PSA process using zeolite 13X as an adsorbent and operated with four steps (pressurization, adsorption, depressurization, and regeneration) is formulated by using PDAEs that consider the dynamic variation and spatial distribution of properties within the adsorption column. For the optimization, we adopt the SD model instead of the CD model and set the CSS condition as the constraint with a small tolerance ($\epsilon$) in the gPROMS modeling system. The decision variables are the bed length, feed pressure, purge pressure, gas velocity, and each operating step time, which are determined to optimize desired objective functions. The objective here is to maximize the purities of $N_2$ and $CO_2$. In the PSA system using zeolite 13X, the optimization results show that the optimal feed pressure should not be high, while other adsorbents such as zeolite 5A require a high feed pressure to obtain a high-purity product.[9,10] Consequently, the PSA process using zeolite 13X can give us a high purity of the components with low energy cost.

Finally, this paper focuses on the optimization of the bench-scale PSA model. In future work, the scale-up of this model will be performed and economic objectives will also be treated.

## Acknowledgment

This research was funded by the Department of Energy through the National Energy Technology Laboratory (NETL).

## Nomenclature

$a_i$, $b_i$ = Langmuir constants (1/Pa)
$C_{pg}$ = heat capacity of the gas (J/kg/K)
$C_{ps}$ = heat capacity of the adsorbent (J/kg/K)
$D_e$ = effective diffusivity ($m^2$/s)
$D_{particle}$ = particle diameter (m)
$D_x$ = dispersion coefficient ($m^2$/s)
$h_i$ = heat-transfer coefficient (J/$m^2$/s/K)
$i$ = component identifier ($i$ = 1 denotes $CO_2$, and $i$ = 2 is $N_2$)
$k_a$ = parameter calculated for the initial condition to satisfy the CSS condition
$k_b$ = parameter calculated for the initial condition to satisfy the CSS condition
$k_c$ = parameter calculated for the initial condition to satisfy the CSS condition
$k_d$ = parameter calculated for the initial condition to satisfy the CSS condition
$K_L$ = effective axial thermal conductivity (J/m/s/K)
$P$ = total pressure (Pa)
$P_{feed}$ = feed pressure (Pa)
$P_i$ = partial pressure (Pa)
$P_{purge}$ = purge pressure (Pa)
$q_i$ = solid-phase concentration (mol/kg)
$q_i^*$ = amount of adsorption of component $i$ in the equilibrium state of the mixture
$R$ = universal gas constant (J/mol/K)
$R_{bed}$ = bed radius (m)
$R_{particle}$ = particle radius (m)
$t$ = time (s)
$t_{cycle}$ = cycle time (s)
$t_P$ = pressurization time (s)
$t_A$ = adsorption time (s)
$t_{DP}$ = depressurization time (s)
$t_R$ = regeneration time (s)
$T$ = gas temperature within the bed (K)
$T_{wall}$ = column wall temperature (K)
$u$ = superficial gas velocity (m/s)
$u_{feed}$ = feed gas velocity (m/s)
$u_{reg}$ = regeneration gas velocity (m/s)
$y_f$ = feed mole fraction
$y_i$ = mole fraction of component $i$
$z$ = axial position (m)

*Greek Letters*

$\epsilon$ = small value
$\mu$ = gas viscosity (kg/m/s)
$\rho_{bed}$ = bed density (kg/$m^3$)
$\epsilon_{bed}$ = bed void
$\rho_{gas}$ = gas density (kg/$m^3$)
$\Delta H_i$ = isosteric heat of adsorption (J/mol) of component $i$
$\rho_{particle}$ = particle density (kg/$m^3$)
$\epsilon_t$ = total void fraction

## Literature Cited

(1) Ruthven, D. M.; Farooq, S.; Knaebel, K. S. *Pressure Swing Adsorption*; VCH Publishers: New York, 1994.

(2) Yang, R. T. *Gas separation by adsorption processes*; Butterworth: Boston, 1987.

(3) Bitzer, M.; Zeitz, M. Process control scheme for a 2-bed pressure swing adsorption plant. In *European Symposium on Computer Aided Process Engineering—12*; Grievink, J., van Schijndel, J., Eds.; Computer-Aided Chemical Engineering; Elsevier Science: New York, 2002; Vol. 10, pp 451−456.

(4) Croft, D. T.; Levan, M. G. Periodic states of adsorption cycles—I. Direct determination and stability. *Chem. Eng. Sci.* **1994**, *49* (11), 1821−1829.

(5) Kvamsdal, H. M.; Hertzberg, T. Optimization of PSA systems—studies on cyclic steady-state convergence. *Comput. Chem. Eng.* **1997**, *21* (8), 819−832.

(6) Smith, O. J.; Westerberg, A. W. Acceleration of cyclic steady-state convergence for pressure swing adsorption models. *Ind. Eng. Chem. Res.* **1992**, *31*, 1569−1573.

(7) Smith, O. J., IV; Westerberg, A. W. Mixed-integer programming for pressure swing adsorption cycle scheduling. *Chem. Eng. Sci.* **1990**, *45* (9), 2833−2842.

(8) Smith, O. J.; Westerberg, A. W. The optimal design of pressure swing adsorption systems. *Chem. Eng. Sci.* **1991**, *46*, 2967−2976.

(9) Nilchan, S.; Pantelides, C. C. On the optimisation of periodic adsorption processes. *Adsorption—J. Int. Adsorpt. Soc.* **1998**, *4*, 113−147.

(10) Cheng, Y. S.; Abi, C. F.; Kershenbaum, L. S. On-line estimation for a fixed-bed reactor with catalyst deactivation using nonlinear programming techniques. *Comput. Chem. Eng.* **1989**, *20*, S793−S798.

(11) Ko, D.; Moon, I. Multiobjective Optimization of cyclic adsorption processes. *Ind. Eng. Chem. Res.* **2002**, *41* (1), 93−104.

(12) Nilchan, S. The optimisation of periodic adsorption processes. Ph.D. Thesis, University of London, London, U.K., 1997.

(13) Yongsunthon, I. Design of periodic adsorptive reactors for the optimal integration of reaction, separation and heat-exchange. Ph.D. Thesis, University of London, London, U.K., 1999.

(14) Yongsunthon, I.; Alpay, E. Design and optimization of temperature cycled adsorptive reactors. *Comput. Chem. Eng.* **1998**, *22*, S733−736.

(15) Lewandowski, J.; Lemcoff, N. O.; Palosaari, S. Use of neural networks in the simulation and optimization of pressure swing adsorption processes. *Chem. Eng. Technol.* **1998**, *21*, 593−597.

(16) Jiang, L.; Biegler, L. T.; Fox, V. G. Simulation and Optimization of Pressure Swing Adsorption Systems for Air Separation. **2002**, submitted for publication.

(17) Siriwardane, R. Sorbent Development for $CO_2$ Separation and Removal: Pressure Swing & Temperature Swing Adsorption. Merit review, NETL, Feb 12, 2002.

(18) Kumar, R.; Fox, V. G.; Hartzog, D. G.; Larson, R. E.; Chen, Y. C.; Houghton, P. A.; Naheiri, T. A Versatile Process Simulator for Adsorptive Separations. *Chem. Eng. Sci.* **1994**, *49*, 3115−3125.

(19) Barton, P. I. The Modelling and Simulation of Combined Discrete/Continuous Processes. Ph.D. Thesis, University of London, London, U.K., 1992.

(20) Oh, M. Modelling and Simulation of Combined Lumped and Distributed Processes. Ph.D. Thesis, University of London, London, U.K., 1995.

(21) Schiesser, W. E. *The Numerical Method of Lines*; Academic Press: New York, 1991.

(22) Jarvis, R. B. Robust Dynamic Simulation of Chemical Engineering Processes. Ph.D. Thesis, University of London, London, U.K., 1993.

(23) Chen, C. L.; Macchietto, S. Technical Report, Centre for Process Systems Engineering, University of London, London, U.K., 1989.

(24) Cheng, Y. S.; Alpay, E.; Kershenbaum, L. S. Simulation and optimization of a rapid pressure swing reactor. *Comput. Chem. Eng.* **1998** Suppl. 22, S45−S52.

*Received for review* June 17, 2002
*Revised manuscript received* September 16, 2002
*Accepted* September 25, 2002